Reduced-Complexity Baseband Compensation of Joint Tx/Rx I/Q Imbalance in Mobile MIMO-OFDM

Balachander Narasimhan, *Student Member, IEEE,* Sudharsan Narayanan, *Student Member, IEEE,* Hlaing Minn, *Senior Member, IEEE,* and Naofal Al-Dhahir, *Fellow, IEEE*

***Abstract*—Direct-conversion multiple-input multiple-output orthogonal frequency division multiplexing (MIMO-OFDM) transceivers enjoy high data rates and reliability at practical implementation complexity. However, analog front-end impairments such as I/Q imbalance and high mobility requirements of next-generation broadband wireless standards result in performance-limiting inter-carrier interference (ICI). In this paper, we study the effects of ICI due to these impairments for OFDM with space frequency block codes and spatial multiplexing, derive a generalized linear model and propose a non-iterative reduced-complexity digital baseband joint compensation scheme. Furthermore, we present a pilot scheme for joint estimation of the channel and the I/Q imbalance parameters and evaluate its performance through simulations. Our proposed scheme is effective in estimating and compensating for frequency-independent and frequency-dependent transmit and receive I/Q imbalances even in the presence of a residual frequency offset.**

***Index Terms*—OFDM, MIMO, I/Q imbalance, MMSE, equalization, mobility, ICI.**

I. Introduction

To provide high data rates at practical transceiver complexity, virtually all broadband wireless systems use OFDM, as evident from standards such as Worldwide Interoperability for Microwave Access (WiMAX), Long Term Evolution (LTE), European Digital Video Broadcasting-Terrestrial (DVB-T) and Mobile Broadband Wireless Access (MBWA). However, OFDM is very sensitive to synchronization errors and Radio Frequency (RF) front-end impairments. Moreover, mobile broadband wireless standards require high mobility support, e.g., 120 km/h in WiMAX, 250 km/h in MBWA, and 500 km/h in LTE for some frequencies.

MIMO-OFDM systems provide huge capacity improvements but they employ multiple RF transceiver front-ends increasing system cost and complexity. Direct conversion transceivers, relieving the complexity and cost issues, are particularly attractive for MIMO, but they suffer from several RF impairments such as in-phase/quadrature (I/Q) imbalance and carrier frequency offset (CFO). I/Q imbalance could be frequency-independent (FI) or frequency-dependent (FD) and causes interference between image frequency components. Another form of ICI among sub-carriers is caused by CFO or the relative motion between the transmitter and receiver. These ICI components cause high error floors, hence severely limiting the performance of MIMO-OFDM systems. Therefore, I/Q imbalance is even more important an issue in MIMO than in single-input single-output (SISO) systems. Moreover, the RF front-ends of different antennas may not have the same characteristics, which increases the number of parameters to be estimated and in this paper we provide a generalized scheme for their estimation and compensation.

In [1], we derived a generalized model for FD joint transmitter/receiver (Tx/Rx) I/Q imbalance in a SISO-OFDM system under high mobility and presented low-complexity channel estimation and compensation algorithms. In the literature, [2]–[9] address the issue of I/Q imbalance in MIMO-OFDM systems. None of these papers addresses the issue of mobility. While [10] addresses the issue of I/Q imbalance along with mobility and CFO, the paper considers only SISO systems. References [2]–[4] analyze and compensate I/Q imbalance in space time block coding (STBC)-OFDM schemes which assume the channel to be constant over two or more OFDM symbols. This assumption does not hold for highly mobile OFDM systems. The second class of multiple-antenna techniques for mobile MIMO-OFDM systems is spatial multiplexing (SM)-OFDM, studied in [5]–[8]. While [5] deals with the FI I/Q imbalance case, [7] models FD imbalance only at the receiver side. Although [8] accounts for FD I/Q imbalance on both sides as well as CFO, it does not account for mobility which drastically impacts system design. In this paper, we propose the use of space frequency block coding (SFBC) for mobile OFDM systems with FD I/Q imbalance at both the transmitter and receiver. Since the ICI due to mobility results in interference within an SFBC code block, we propose a "super-block" structure for the Alamouti SFBC. The super-block structure ensures the orthogonality of the Alamouti block in spite of the impairments. Hence, detection can be performed at reasonable complexity while still realizing spatial and multipath diversity gains. Furthermore, we compare SFBC-OFDM and SM-OFDM systems in the presence of high mobility and I/Q imbalance. In both cases, we use

Manuscript received June 5, 2009; revised September 30, 2009; accepted January 20, 2010. The associate editor coordinating the review of this paper and approving it for publication was A. Hjørungnes.

B. Narasimhan, H. Minn, and N. Al-Dhahir are with the Department of Electrical Engineering, University of Texas at Dallas, MSEC33, Richardson, TX, 75080 (e-mail: {bxn062000, Hlaing.Minn, aldhahir}@utdallas.edu).

S. Narayanan was with the University of Texas at Dallas at the time of this writing. He is now with ST-Ericsson, Bangalore, India.

This work is supported by a gift from Research in Motion Inc.

This work was presented in part at CISS 2009.

Digital Object Identifier 10.1109/TWC.2010.05.090847

$$\boldsymbol{\gamma}^{(1)}(k,l) = \begin{bmatrix} \lambda_r(k)\lambda_t(l)g(k,l) + \phi_r(k)\phi_t^*(l')g^*(k',l'), & \lambda_r(k)\phi_t(l)g(k,l) + \phi_r(k)\lambda_t^*(l')g^*(k',l') \\ \lambda_r^*(k')\phi_t^*(l')g^*(k',l') + \phi_r^*(l')\lambda_t(l)g(k,l), & \lambda_r^*(l')\lambda_t^*(l')g^*(k',l') + \phi_r^*(k')\phi_t(l)g(k,l) \end{bmatrix}$$
$$\boldsymbol{\gamma}^{(2)}(k,l) = \begin{bmatrix} \lambda_r(k)\phi_t(l')g(k,l') + \phi_r(k)\lambda_t^*(l)g^*(k',l), & \lambda_r(k)\lambda_t(l')g(k,l') + \phi_r(k)\phi_t^*(l)g^*(k',l) \\ \lambda_r^*(k)\lambda_t^*(l)g^*(k',l) + \phi_r^*(k')\phi_t(l')g(k,l'), & \lambda_r^*(k')\phi_t^*(l)g^*(k',l) + \phi_r^*(k')\lambda_t(l')g(k,l') \end{bmatrix} \quad (1)$$

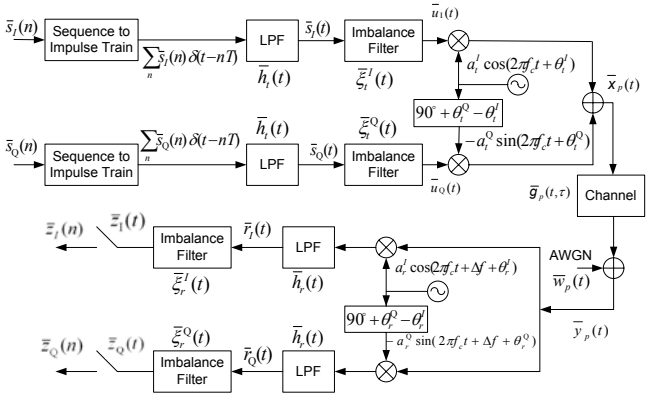

Fig. 1. Block diagram of the joint Tx/Rx I/Q imbalance, residual CFO and mobility model.

low-complexity non-iterative linear MMSE decoding because ICI effects result in a high-dimensional signal vector and, hence, maximum-likelihood (ML) methods are prohibitively complex. Moreover, we show that both our compensation and channel estimation schemes are quite robust to residual CFO.

The rest of this paper is organized as follows. In Section II, we review the SISO joint I/Q imbalance and mobility model in [1]. In Section III, we discuss the design of SFBC and SM encoding schemes and derive their input-output models. In Section IV, we present the linear digital baseband MMSE compensation scheme, and in Section V, we discuss the pilot-aided channel estimation schemes. We extend the model to include CFO effects in Section VI. In Section VII, we present techniques to reduce computational complexity. Finally, we discuss simulation results in in Section VIII.

Notation: All time-domain quantities $\{\bar{x}(t), \bar{\mathbf{x}}, \bar{\mathbf{X}}\}$ have a bar whereas frequency-domain quantities $\{x(f), \mathbf{x}, \mathbf{X}\}$ do not. Vectors $\{\bar{\mathbf{x}}, \mathbf{x}\}$ are represented by lower-case and matrices $\{\bar{\mathbf{X}}, \mathbf{X}\}$ by upper-case boldface letters. $(\cdot)^H$, $(\cdot)^T$ and $(\cdot)^*$ denote respectively the hermitian, transpose and conjugate operations. $\mathbf{F}$ denotes the unitary DFT matrix. Linear convolution is denoted by $\otimes$ while circular convolution modulo-N is by $\circledast_N$. $\mathbf{0}_{m\times n}$ is the all-zero $m \times n$ matrix. The operator diag$(\cdot)$ when applied to a matrix gives a vector containing the diagonal elements of the matrix and when it acts on a vector yields a diagonal matrix whose diagonal elements are the elements of the vector. The operator tr(.) denotes the trace of a matrix.

II. System model and Assumptions

FI I/Q imbalance is caused by oscillator amplitude and phase mismatches at the mixer. Let $\tilde{\alpha}_t$ be the amplitude mismatch and θ_t be the phase mismatch at the transmitter. We define the following I/Q imbalance parameters

$$\mu_t = \left(\cos\frac{\theta_t}{2} - j\tilde{\alpha}_t \sin\frac{\theta_t}{2}\right), \quad \nu_t = \left(\tilde{\alpha}_t \cos\frac{\theta_t}{2} - j\sin\frac{\theta_t}{2}\right).$$

FD I/Q imbalance is caused by the non-ideal and mismatched frequency responses of the LPF's on the I and Q branches, whose frequency responses are $\xi_t^I(k)$ and $\xi_t^Q(k)$, respectively, for $k = 0, \cdots, N-1$ where N is the OFDM FFT size. Define

$$\lambda_t(k) = \frac{1}{2}\Big((\mu_t + \nu_t)\xi_t^I(k) + (\mu_t - \nu_t)\xi_t^Q(k)\Big)$$
$$\phi_t(k) = \frac{1}{2}\Big((\mu_t + \nu_t)\xi_t^I(k) - (\mu_t - \nu_t)\xi_t^Q(k)\Big).$$

In a similar manner, we can define the receiver-side parameters $\tilde{\alpha}_r, \theta_r, \mu_r, \nu_r, \xi_r^I(k), \xi_r^Q(k)$ and

$$\lambda_r(k) = \frac{1}{2}\Big((\mu_r + \nu_r^*)\xi_r^I(k) + (\mu_r - \nu_r^*)\xi_r^Q(k)\Big)$$
$$\phi_r(k) = \frac{1}{2}\Big((\nu_r + \mu_r^*)\xi_r^I(k) + (\nu_r - \mu_r^*)\xi_r^Q(k)\Big).$$

All of these parameters have been labeled in the block diagram in Fig. 1. Now, let the transmitted signal on sub-carrier k be $s(k)$ and the time-varying channel be characterized by $g(k,l)$ where this frequency-domain quantity represents the interference due to sub-carrier l at sub-carrier k. For all k, these ICI terms are collected into the matrix $\mathbf{G}$. Furthermore, define the matrix $\mathbf{\Lambda}_t = \text{Diag}([\lambda_t(0), \cdots, \lambda(N-1)])$ and the matrices $\mathbf{\Phi}_t, \mathbf{\Lambda}_r, \mathbf{\Phi}_r$ corresponding to quantities $\phi_t(k), \lambda_r(k), \phi_r(k)$. As we showed in [1], the received signal is given by

$$\mathbf{z} = \underbrace{(\mathbf{\Lambda}_r\mathbf{G}\mathbf{\Lambda}_t + \mathbf{\Phi}_r\mathbf{G}^{\#}\mathbf{\Phi}_t^{\#})}_{\mathbf{\Psi}^{(1)}}\mathbf{s} + \underbrace{(\mathbf{\Lambda}_r\mathbf{G}\mathbf{\Phi}_t + \mathbf{\Phi}_r\mathbf{G}^{\#}\mathbf{\Lambda}_t^{\#})}_{\mathbf{\Psi}^{(2)}}\mathbf{s}^{\#} + \mathbf{v} \quad (2)$$

where $\mathbf{s} = [s(0), \cdots, s(N-1)]^T$, $\mathbf{z} = [z(0), \cdots, z(N-1)]^T$ and $\mathbf{v} = [v(0), \cdots, v(N-1)]^T$ are the transmitted, received and noise vectors, respectively. Here, the k-th element of $\mathbf{b}^{\#}$ is the conjugate of the $(N-k)$ element of $\mathbf{b}$ and the (n,k) element of $\mathbf{B}^{\#}$ is the conjugate of the $(N-n, N-k)$ element of $\mathbf{B}$. If we write down expressions for each individual term $z(k)$ in (2), we can see that the effect of I/Q imbalance is to cause interference between a sub-carrier k and its image $k' = N-k$ after being weighed by I/Q imbalance parameters. We showed in [1] that for each sub-carrier pair (k,k') $\forall k = 1, \cdots, \frac{N}{2} - 1$, we can write

$$\mathbf{z}(k) = \sum_{l=0}^{\frac{N}{2}-1}\Big(\boldsymbol{\gamma}^{(1)}(k,l)\mathbf{s}(l) + \boldsymbol{\gamma}^{(2)}(k,l)\mathbf{s}(l)^*\Big) + \mathbf{v}(k) \quad (3)$$

where $\mathbf{z}(k) = [z(k), z^*(k')]^T$, $\mathbf{s}(l) = [s(l), s^*(l')]^T$, $\mathbf{v}(k) = [v(k), v^*(k')]^T$ and the $\boldsymbol{\gamma}^{(\cdot)}(k,l)'s$ are as defined in (1).

We showed in [1] that the term $\boldsymbol{\gamma}^{(2)}(k,l)$ can be ignored. Moreover, the effect of ICI due to mobility can be considered significant only on a few, say D, adjacent sub-carriers. With

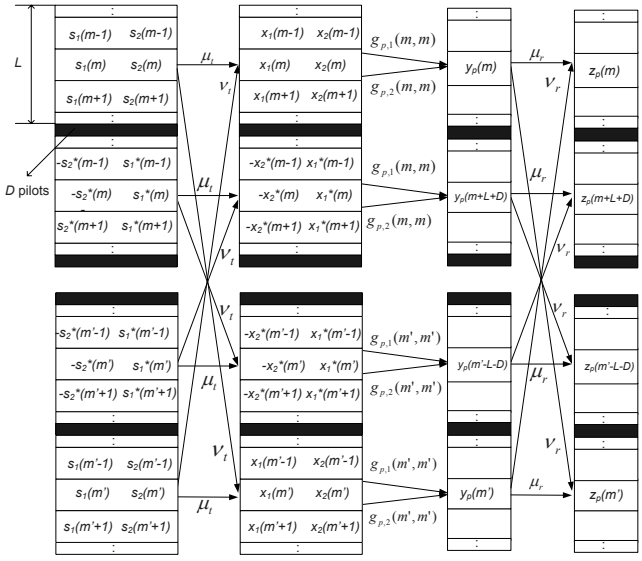

Fig. 2. Proposed super-block structure for Alamouti SFBC-OFDM.

these approximations, (3) can be simplified as

$$\mathbf{z}(k) = \sum_{l=-D}^{D} \boldsymbol{\gamma}^{(1)}(k,l)\mathbf{s}(l) + \mathbf{v}(k). \tag{4}$$

For brevity, we define $\boldsymbol{\gamma}^{(1)}(k,l) \triangleq \begin{bmatrix} g^a(k,l) & (g^b(k',l'))^* \\ g^b(k,l) & (g^a(k,l))^* \end{bmatrix}$.

III. System Models for MIMO Transmission

A. Alamouti SFBC

We focus on the Alamouti SFBC for two transmit antennas due to its popularity and its wide-spread adoption in standards[1]. Denoting the number of receive antennas by N_P, our proposed scheme is shown in Fig. 2. It uses the super-block structure described in [12]. In conventional SFBC OFDM, one Alamouti code-block occupies two adjacent sub-carriers and in the presence of mobility, it would result in intra-code-block interference which destroying the orthogonality and performance of the Alamouti code. With our proposed super-block structure, this intra-code-block interference is significantly reduced. Moreover, it results in an elegant linear model that could be estimated and equalized with low complexity. Now, to deal with I/Q imbalance, we position two super-blocks such that they occupy sub-carriers that are exactly images of each other. For example, if super-block $\mathcal{S}_b$ occupies sub-carriers k_b to $k_b + (2L + 2D - 1)$, the image super-block $\mathcal{S}_{b'}$ occupies sub-carriers $k_b' - (2L + 2D - 1)$ to k_b' where $k_b' = N - k_b$. Here k_b is the index of the first sub-carrier of superblock S_b, L is the number of Alamouti SFBC blocks within the super-block and $2D$ is the number of pilots, so that the length of the super-block is $2(L + D)$, where D is chosen according to the extent of ICI caused by mobility. The super-blocks are arranged symmetrically with respect to the DC sub-carrier.

Within a super-block S_b, there are L code-blocks and the symbols within these code-blocks are labeled as $\{s_1(m)s_2(m); m = 0, \cdots, L-1\}$[2]. The Alamouti code-block m is formed by transmitting symbols $s_1(m)$ and $s_2(m)$, respectively, from Antennas 1 and 2 of Sub-carrier $(k_b + m)$ and transmitting symbols $-s_2^*(m)$ and $s_1^*(m)$, respectively, from Antennas 1 and 2 of Sub-carrier $(k_b + m + L + D)$. Sub-carriers $(k_b + L)$ to $(k_b + L + D - 1)$ are occupied by pilots. This aids in separating the first-slot Alamouti code symbols $\{s_1(m), s_2(m)\}$ from the second-slot Alamouti code symbols $\{-s_2^*(m), s_1^*(m)\}$, thus resulting in the elegant linear model with the Alamouti block structure derived in this section.

The mobility-induced ICI coefficient at Sub-carrier m due to Sub-carrier n is denoted by $g_{p,q}(m,n)$ where p and q are the receiver and transmitter antenna indices, respectively. $g_{p,q}(m,m)$ represents the gain at Sub-carrier m. It should be noted that, even for a significant Doppler, with the choice of a large L, interference among sub-carriers from different super-blocks is negligible. Moreover, it is assumed that $g_{p,q}(m,n) \approx g_{p,q}(m+L+D, n+L+D)\ \forall m$ and $(m-n)$ fixed. For this assumption to hold, L has to be chosen along with D such that $(L + D)$ sub-carriers lie within the coherence bandwidth of the channel. Under this assumption, using (4), and taking the necessary conjugates, we can write the received symbol vector $\mathbf{z}_p(m) = [z_p(m)\ z_p^*(m+L+D)\ z_p^*(m'-L-D)\ z_p(m')]^T$ belonging to super-blocks S_b and $S_{b'}$ at receiver antenna p as

$$\mathbf{z}_p(m) = \sum_{n=m-D}^{m+D} \mathbf{G}_p(m,n)\mathbf{s}(n) + \mathbf{v}_p(m) \tag{6}$$

where $\mathbf{s}(m) = [s_1(m)\ s_2(m)\ s_1^*(m')\ s_2^*(m')]^T$, $\mathbf{v}_p(m) = [v_p(m)\ v_p^*(m+L+D)\ v_p^*(m'-L-D)\ v_p(m')]^T$ and $\mathbf{G}_p(m,n)$ is defined in (5). The quantities in $\mathbf{G}_p(m,n)$ are defined as

$$\begin{aligned} g_{p,q}^a(m,n) &\triangleq \lambda_{r,p}(m)\lambda_{t,q}(n)g_{p,q}(m,n) \\ &\quad +\phi_{r,p}(m)\phi_{t,q}^*(n')g_{p,q}^*(m',n') \\ g_{p,q}^b(m,n) &\triangleq \lambda_{r,p}^*(m')\phi_{t,q}^*(n')g_{p,q}^*(m',n') \\ &\quad +\phi_{r,p}^*(m')\lambda_{t,q}(n)g_{p,q}(m,n). \end{aligned} \tag{7}$$

Equation (6) for different p's can be combined together to obtain the following model

$$\underbrace{\begin{bmatrix} \mathbf{z}_0(m) \\ \mathbf{z}_1(m) \\ \vdots \\ \mathbf{z}_{N_P-1}(m) \end{bmatrix}}_{\mathbf{z}(m)} = \sum_{n=m-D}^{m+D} \underbrace{\begin{bmatrix} \mathbf{G}_0(m,n) \\ \mathbf{G}_1(m,n) \\ \vdots \\ \mathbf{G}_{N_P-1}(m,n) \end{bmatrix}}_{\mathbf{G}(m,n)} \mathbf{s}(n) + \underbrace{\begin{bmatrix} \mathbf{v}_0(m) \\ \mathbf{v}_1(m) \\ \vdots \\ \mathbf{v}_{N_P-1}(m) \end{bmatrix}}_{\mathbf{v}(m)}. \tag{8}$$

In (8), $\mathbf{G}(m,n)$ represents a block that accounts for all the I/Q imbalance effects and we denote its size by $B_r \times B_c$ which in the Alamouti SFBC case is equal to $4N_P \times 4$ and comprised of $\mathbf{G}_p(m,n)$'s which are, in turn, composed of Alamouti blocks as shown in (5). It is interesting to see that although the system order has increased and image components interfere with each other, the Alamouti block structure is still retained because of the super-block arrangement. In Section VII, we will show how to exploit this Alamouti block structure to achieve significant savings in computational complexity.

[1]Extensions to other SFBC schemes based on orthogonal designs[11] are straightforward.

[2]The subscripts 1 and 2 are not transmit antenna indices. Also, there is no explicit super-block indexing for convenience of notation.

$$\mathbf{G}_p(m,n) = \left[\begin{array}{cc|cc} g^a_{p,1}(m,n) & g^a_{p,2}(m,n) & (g^b_{p,1}(m',n'))^* & (g^b_{p,2}(m',n'))^* \\ (g^a_{p,2}(m,n))^* & -(g^a_{p,1}(m,n))^* & g^b_{p,2}(m',n') & -g^b_{p,1}(m',n') \\ \hline g^b_{p,1}(m,n) & g^b_{p,2}(m,n) & (g^a_{p,1}(m',n'))^* & (g^a_{p,2}(m',n'))^* \\ (g^b_{p,2}(m,n))^* & -(g^b_{p,1}(m,n))^* & g^a_{p,2}(m',n') & -g^a_{p,1}(m',n') \end{array}\right], \tag{5}$$

B. Spatial Multiplexing

We consider an SM-OFDM system with N_Q transmit and N_P receive antennas with $N_P \geq N_Q$ to enable MMSE linear decoding. The encoding is trivial in that each transmit antenna carries an independent symbol in each sub-carrier. Therefore, we use $s_q(m)$ to denote the symbol transmitted on Antenna-q of Sub-carrier m. Then, using (4), we can write the symbols received on Antenna p of Sub-carriers m and m' as follows

$$\underbrace{\begin{bmatrix} z_p(k) \\ z_p^*(k') \end{bmatrix}}_{\mathbf{z}_p(k)} = \sum_{q=0}^{N_Q-1} \sum_{l=k-D}^{k+D} \underbrace{\begin{bmatrix} g^a_{p,q}(k,l) & (g^b_{p,q}(k,l))^* \\ g^b_{p,q}(k,l) & (g^a_{p,q}(k,l))^* \end{bmatrix}}_{\mathbf{G}_{p,q}(k,l)} \times \underbrace{\begin{bmatrix} s_q(l) \\ s_q^*(l') \end{bmatrix}}_{\mathbf{s}_q(l)} + \underbrace{\begin{bmatrix} v_p(k) \\ v_p^*(k') \end{bmatrix}}_{\mathbf{v}_p(k)}, \tag{9}$$

where the quantities in $\mathbf{G}_{p,q}(k,l)$ have been defined in (7). For N_P receive antennas, (9) generalizes to

$$\underbrace{\begin{bmatrix} \mathbf{z}_0(k) \\ \mathbf{z}_1(k) \\ \vdots \\ \mathbf{z}_{N_P-1}(k) \end{bmatrix}}_{\mathbf{z}(k)} = \sum_{l=k-D}^{k+D} \mathbf{G}(k,l) \underbrace{\begin{bmatrix} \mathbf{s}_0(l) \\ \mathbf{s}_1(l) \\ \vdots \\ \mathbf{s}_{N_Q-1}(l) \end{bmatrix}}_{\mathbf{s}(l)} + \underbrace{\begin{bmatrix} \mathbf{v}_0(k) \\ \mathbf{v}_1(k) \\ \vdots \\ \mathbf{v}_{N_P-1}(k) \end{bmatrix}}_{\mathbf{v}(k)}, \tag{10}$$

where

$$\mathbf{G}(k,l) = \begin{bmatrix} \mathbf{G}_{0,0}(k,l) & \cdots & \mathbf{G}_{0,N_Q-1}(k,l) \\ \vdots & \ddots & \vdots \\ \mathbf{G}_{N_P-1,0}(k,l) & \cdots & \mathbf{G}_{N_P-1,N_Q-1}(k,l) \end{bmatrix}.$$

Equation (10) differs from an SM-OFDM system with no I/Q imbalance in that the channel block-matrix $\mathbf{G}(k,l)$ is of size $B_r \times B_c = 2N_P \times 2N_Q$ rather than $N_P \times N_Q$ and the output at each sub-carrier also depends on the symbols on its image sub-carrier and their neighbors.

IV. Digital Baseband Compensation Scheme

Equations (8) and (10) are similar except for the matrix dimensions and the sub-block structure. In the SFBC case, we used indices (m,n) to represent Alamouti blocks. For convenience, henceforth, we represent both of them using the indices (k,l). Now, in both (8) and (10), it can be seen that for a given D, an input symbol vector $\mathbf{s}(k)$ leaks into vectors $\mathbf{s}(k-D)$ to $\mathbf{s}(k+D)$. Therefore, we need to process $\{\mathbf{z}(k-D), \cdots, \mathbf{z}(k), \cdots, \mathbf{z}(k+D)\}$ to estimate $\mathbf{s}(k)$. With this in mind, we define the following quantities

$$\tilde{\mathbf{z}}(k) \triangleq \begin{bmatrix} \mathbf{z}(k-D) \\ \vdots \\ \mathbf{z}(k) \\ \vdots \\ \mathbf{z}(k+D) \end{bmatrix}, \tilde{\mathbf{s}}(k) \triangleq \begin{bmatrix} \mathbf{s}(k-2D) \\ \vdots \\ \mathbf{s}(k) \\ \vdots \\ \mathbf{s}(k+2D) \end{bmatrix},$$

$$\tilde{\mathbf{v}}(k) \triangleq \begin{bmatrix} \mathbf{v}(k-D) \\ \vdots \\ \mathbf{v}(k) \\ \vdots \\ \mathbf{v}(k+D) \end{bmatrix}, \tilde{\mathcal{G}}(k) \triangleq \begin{bmatrix} \mathbf{G}(k-D,k) \\ \vdots \\ \mathbf{G}(k,k) \\ \vdots \\ \mathbf{G}(k+D,k) \end{bmatrix}$$

and $\tilde{\mathbf{G}}(k)$ is defined in (11) and of size $(2D+1)B_r \times (4D+1)B_c$. Then the linear MMSE estimate of $\mathbf{s}(k)$ is given by

$$\hat{\mathbf{s}}(k) = \tilde{\mathbf{w}}^H(k)\tilde{\mathbf{z}}(k) \tag{12}$$

where $\tilde{\mathbf{w}}^H(k) = \tilde{\mathcal{G}}^H(k)\left(\tilde{\mathbf{G}}(k)\tilde{\mathbf{G}}^H(k) + \frac{1}{\mathrm{SNR}}\mathbf{I}_{(2D+1)B_r}\right)^{-1} = [\mathbf{w}^H(k-D)\cdots\mathbf{w}^H(k)\cdots\mathbf{w}^H(k+D)]$ and each of the $\mathbf{w}^H(k)$'s is of size 2×2. It should be noted that $\mathbf{s}(k)$ consists of $2N_Q$ symbols. Therefore, the application of (12) to each k results in the estimation of $2N_Q$ transmitted symbols. Moreover, $\tilde{\mathbf{z}}(k)$ is of size $(2D+1)B_r$ which for $D=1$ and $N_P = N_Q = 2$ is equal to 24 for SFBC and 12 for SM. However, the symbols for one SFBC code block are spread over two sub-carriers while those for the SM code block are over just one sub-carrier. Hence, only six taps per sub-carrier are needed to detect a code block when $D=1$.

V. Channel Estimation

Equation (4) represents a linear model wherein the channel and I/Q imbalance parameters are combined, so that we can perform linear estimation keeping the number of parameters small. There are four parameters (in each $\boldsymbol{\gamma}^{(1)}(k,l)$) to be estimated for each transmit-receive antenna pair. However, there are $(2D+1)$ terms in the summation in (4) and, hence, a total of $4(2D+1)$ parameters. Note that $\boldsymbol{\gamma}^{(1)}(k,l)$'s for $l=k$ represent the channel gain for the sub-carrier pair $\{k, N-k\}$ and the rest of the terms ($l \neq k$) represent the ICI. Moreover, the $\boldsymbol{\gamma}^{(1)}(k,k)$'s are the diagonal elements of $\boldsymbol{\Psi}^{(1)}$ and $\boldsymbol{\Psi}^{(2)}$ and in general, they are much larger than their respective off-diagonal ones. Therefore, we ignore the non-diagonal terms and estimate only the diagonal terms.

Next, we describe the pilot scheme, which is valid for both FI and FD I/Q imbalances. Equation (4) involves a sub-carrier and its image. Therefore, it makes sense to assign pilots in image locations. Since there are four parameters and, we assign a pair of pilots on each side of the DC sub-carrier for each transmit antenna. At any pilot location, only one of the antennas is excited with pilots and the others are switched off, so that the sequences are orthogonal across the antennas satisfying the criterion for optimality in [13]. The pilot patterns for SFBC and SM are shown in Figs. 3(a) and 3(b), respectively. In case of SFBC, the pilot pair on each side is not contiguous because of the super-block structure. At receive antenna p, we need to estimate $\mathbf{g}_{p,q}(k,k)$. Assume that we excite Antenna q with a pilot quadruple on sub-carriers k_1, k_2, k_2', k_1', where $k_2 = k_1 + L + D$ for SFBC and $k_2 = k_1 + 1$ for SM. Then, for sub-carrier pair $\{k_1, k_1'\}$

$$\tilde{\mathbf{G}}(k) \triangleq \begin{bmatrix} \mathbf{G}(k-D,k-2D) & \cdots & \mathbf{G}(k-D,k-D) & \cdots & \mathbf{G}(k-D,k) & \cdots & \mathbf{0} \\ & \ddots & & \ddots & & & \\ \vdots & \mathbf{G}(k,k-D) & \cdots & \mathbf{G}(k,k) & \cdots & \mathbf{G}(k,k+D) & \vdots \\ & & \ddots & & \ddots & & \\ \mathbf{0} & \cdots & \mathbf{G}(k+D,k) & \cdots & \mathbf{G}(k+D,k+D) & \cdots & \mathbf{G}(k+D,k+2D) \end{bmatrix}, \quad (11)$$

$$\begin{bmatrix} z_p(k_1) \\ z_p^*(k_1') \end{bmatrix} = \begin{bmatrix} g_{p,q}^a(k_1,k_1) & (g_{p,q}^b(k_1',k_1'))^* \\ g_{p,q}^b(k_1,k_1) & (g_{p,q}^a(k_1',k_1'))^* \end{bmatrix} \times \begin{bmatrix} s_q(k_1) \\ s_q^*(k_1') \end{bmatrix} + \begin{bmatrix} v_q(k_1) \\ v_q^*(k_1') \end{bmatrix}, \quad (13)$$

and we can write a similar equation for the sub-carrier pair $\{k_2, k_2'\}$. Now, since we assumed $\mathbf{g}_{p,q}(k_1,k_1) = \mathbf{g}_{p,q}(k_2,k_2)$, the equations for the two pairs can be combined as

$$\underbrace{\begin{bmatrix} z_p(k_1) \\ z_p^*(k_1') \\ z_p(k_2) \\ z_p^*(k_2') \end{bmatrix}}_{\mathbf{z}(k_1)} = \underbrace{\begin{bmatrix} s_q(k_1) & 0 & s_q^*(k_1') & 0 \\ 0 & s_q^*(k_1') & 0 & s_q(k_1) \\ s_q(k_2) & 0 & s_q^*(k_2') & 0 \\ 0 & s_q^*(k_2') & 0 & s_q(k_2) \end{bmatrix}}_{\mathcal{S}(k_1)} \times \underbrace{\begin{bmatrix} g_{p,q}^a(k_1,k_1) \\ (g_{p,q}^a(k_1',k_1'))^* \\ (g_{p,q}^b(k_1',k_1'))^* \\ g_{p,q}^b(k_1,k_1) \end{bmatrix}}_{\mathbf{g}(k_1)} + \begin{bmatrix} v_q(k_1) \\ v_q^*(k_1') \\ v_q(k_2) \\ v_q^*(k_2') \end{bmatrix}. \quad (14)$$

We perform least-squares (LS) estimation of the channel and, hence, we require that the trace $\mathrm{tr}(\mathcal{S}^H(k_1)\mathcal{S}(k_1)) = \sigma_p^2 \mathbf{I}_4$ for the LS error to be minimum [14]. Here, σ_p^2 corresponds to the power constraint on the pilots. In OFDM symbols with both data and pilot sub-carriers, the procedure gives the channel estimates only at the pilot locations. We use a DFT based interpolation scheme that gives the time-domain channel taps from the frequency-domain channel coefficients available at the pilot locations. Let $\mathbf{g}_{p,q}^a$ be the vector that contains all available $g_{p,q}^a(k_1,k_1)$'s with ordered indices. Then, we have

$$\mathrm{diag}(\mathbf{\Psi}_{p,q}^{(1)}) = \mathbf{F}(\tilde{\mathbf{F}}^H\tilde{\mathbf{F}})^{-1}\tilde{\mathbf{F}}^H\mathbf{g}_{p,q}^a \quad (15)$$

where $\tilde{\mathbf{F}}$ is a matrix containing the columns of the DFT matrix that correspond to the pilot locations. Similarly, we collect all the $\mathbf{g}_{p,q}^b$'s together to obtain $\mathrm{diag}(\mathbf{\Psi}_{p,q}^{(2)})$. This way, we have obtained all the diagonal elements. To obtain the non-diagonal elements, we use the method described in [15] which involves linearly interpolating each tap in the time-domain across three consecutive OFDM symbols, and then going back to the frequency domain to obtain the matrices $\mathbf{\Psi}_{p,q}^{(1)}$ and $\mathbf{\Psi}_{p,q}^{(2)}$.

VI. Carrier Frequency Offset

OFDM systems are sensitive to carrier frequency offset (CFO) which is unavoidable because it is difficult to accurately synchronize two remote oscillators (one at the transmitter and the other at the receiver) to the same frequency and phase. The effect of this offset, denoted by Δf in Fig. 1, is to destroy the orthogonality of the sub-carriers thus causing ICI [16]. While Δf is the actual frequency offset in Hertz, we define the more useful quantity $\widetilde{\Delta f} = \frac{N\Delta f}{F_s}$, which is the frequency offset normalized by the sub-carrier spacing. Referring to Fig. 1, where $\bar{y}(n)$ is the received baseband equivalent signal, it can

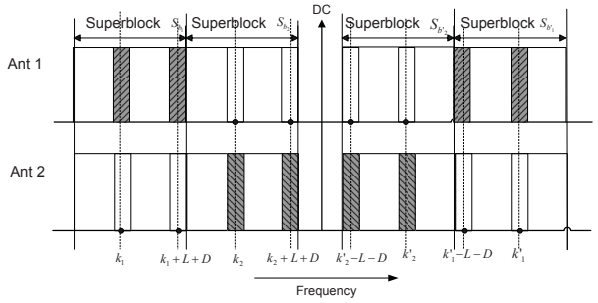

(a) SFBC-OFDM

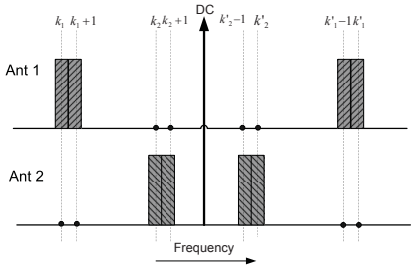

(b) SM-OFDM

Fig. 3. Proposed pilot patterns.

be shown that in the presence of CFO, the equivalent received signal (without considering I/Q imbalance) is not $\bar{y}(n)$ but

$$\bar{y}_{\mathrm{CFO}}(n) = e^{\frac{j2\pi\widetilde{\Delta f}n}{N}}\bar{y}(n). \quad (16)$$

Now, if we define $\bar{\mathbf{\Omega}} = \mathrm{Diag}([1, e^{\frac{j2\pi\widetilde{\Delta f}}{N}}, \cdots, e^{\frac{j2\pi\widetilde{\Delta f}(N-1))}{N}}]^T)$, then we get $\bar{\mathbf{r}} = \bar{\mathbf{\Omega}}\bar{\mathbf{y}}$ and in the frequency domain, $\mathbf{r} = \mathbf{\Omega}\mathbf{y}$, where $\mathbf{\Omega} = \mathbf{F}\bar{\mathbf{\Omega}}\mathbf{F}^H$. Therefore, we can rewrite (2) as

$$\mathbf{z} = (\mathbf{\Lambda}_r\mathbf{G}_\Omega\mathbf{\Lambda}_t + \mathbf{\Phi}_r\mathbf{G}_\Omega^{\#}\mathbf{\Phi}_t^{\#})\mathbf{s} + (\mathbf{\Lambda}_r\mathbf{G}_\Omega\mathbf{\Phi}_t + \mathbf{\Phi}_r\mathbf{G}_\Omega^{\#}\mathbf{\Lambda}_t^{\#})\mathbf{s}^{\#} + \mathbf{v} \quad (17)$$

where $\mathbf{G}_\Omega = \mathbf{\Omega}\mathbf{G}$. Here we assume that the 'residual' CFO confined to within the sub-carrier spacing, i.e., $\widetilde{\Delta f} < 1$. Now $\mathbf{\Omega}$ is a circulant matrix (since $\bar{\mathbf{\Omega}}$ is diagonal) and $\mathbf{G}$ is a banded matrix. However, only a few sub-diagonals on each side of the main diagonal of $\mathbf{\Omega}$ are significant. Therefore, we can set the rest of the elements to be zero, i.e., $\mathbf{\Omega}$ can also be replaced by its banded approximation. Although this increases the number of sub-diagonals in the resulting model, simulation studies show that the compensation schemes proposed in this paper are quite robust to typical residual CFO values as it will be shown in Section VIII. This implies that we do not have to explicitly deal with the CFO problem during compensation and also not explicitly estimate the CFO parameter $\widetilde{\Delta f}$.

VII. Complexity Considerations

The linear MMSE compensation scheme in (12) involves the computation of a Grammian and matrix inversion. For

$D = 1$ with two transmit and two receive antennas, the SM and SFBC schemes require matrix inversions of size 12×12 and 24×24 respectively. However, there are common channel elements in adjacent sub-carriers. Moreover, the Hermitian and Alamouti structure of these matrices allow for further computational reductions, which we would discuss in detail in this section.

If we use the same arguments in [17] for complex Hermitian matrices, it is easy to show that $\frac{M_r^2}{2}$ complex divisions and $\frac{M_r^3}{2}$ complex MAC operations are required to invert them. The computation of the Grammian of a complex matrix of size $M_r \times M_c$ requires $\frac{M_r M_c (M_r+1)}{2}$ complex MAC operations. We have to deal with matrices of size $(2D+1)B_r \times (4D+1)B_c$. Here, $B_r \times B_c$ represents the size of the blocks in matrix $\tilde{\mathbf{G}}(m)$. The Grammian computation would require $\frac{B_r B_s}{2}(2D+1)(4D+1)(2DB_r + B_r + 1)$ complex MAC's and the matrix inversion would require $\frac{(2D+1)^2 B_r^2}{2}$ complex divisions and $\frac{(2D+1)^3 B_r^3}{2}$ complex MAC's. The following techniques help us reduce the computational complexity.

A. Recursive Computation of the Grammian

For both SM and SFBC, the MMSE estimation in (12) involves the computation of the Grammain $\tilde{\mathbb{G}}(m) = \tilde{\mathbf{G}}(m)\tilde{\mathbf{G}}^H(m)$ for $m = 0, \cdots, L-1$. Note that there are several common elements between $\tilde{\mathbf{G}}(m)$ and $\tilde{\mathbf{G}}(m+1)$. $\tilde{\mathbf{G}}(m)$ is a block matrix of size $(2D+1) \times (4D+1)$ blocks and each block-row has only $(2D+1)$ non-zero blocks. As the code-block index increases from m to $m+1$, only one block-row is replaced by a new block-row. Therefore, only one new block-row needs to be computed each time which requires $(2D+1)(D+1)$ block MAC's. The resulting blocks themselves are symmetric and hence $(2D+1)(D+1)\frac{B_r B_c (B_r+1)}{2}$ complex MAC's are needed in computing the Grammian.

B. Recursive Algorithm for Inversion

The other expensive computation step is the inversion of $\tilde{\mathbb{G}}_M(m) = \left(\tilde{\mathbb{G}}(m) + \frac{1}{\mathrm{SNR}}\mathbf{I}\right)$. For this, we consider two different ways of partitioning the block-Hermitian matrix $\tilde{\mathbb{G}}(m)$ as shown in (18) where each $\times$ represents a block of size $B_r \times B_c$. Consider the inversion formulae (19) and (20)[3] for $\tilde{\mathbb{G}}(m)$ [18], where $\mathbf{\Delta}_l(m) = \mathbf{A}_l(m) - \mathbf{B}_l(m)\mathbf{D}_l^{-1}(m)\mathbf{C}_l(m)$ and $\mathbf{\Delta}_u(m) = \mathbf{D}_u(m) - \mathbf{C}_u(m)\mathbf{A}_u^{-1}(m)\mathbf{B}_u(m)$. Since $\tilde{\mathbb{G}}(m)$ is Hermitian, $\tilde{\mathbb{G}}^{-1}(m)$ is also Hermitian and hence $\mathbf{R}_l(m) = \mathbf{Q}_l^H(m)$ and $\mathbf{R}_u(m) = \mathbf{Q}_u^H(m)$. Moreover, with the partitioning in two different ways, we see that $\mathbf{D}_l(m) = \mathbf{A}_u(m+1)$. Suppose that $\tilde{\mathbb{G}}^{-1}(m)$ has been computed, then $\tilde{\mathbb{G}}^{-1}(m+1)$ is computed using the following steps.

1) Compute $\mathbf{\Delta}_l(m)$ by inverting $\mathbf{\Delta}_l^{-1}(m)$
2) Compute $\mathbf{D}_l^{-1}(m) = \mathbf{S}_l(m) - \mathbf{Q}_l^H(m)\mathbf{\Delta}_l(m)\mathbf{Q}_l(m)$.
3) Now $\mathbf{A}_u^{-1}(m+1) = \mathbf{D}_l^{-1}(m)$. Compute $\tilde{\mathbb{G}}^{-1}(m+1)$ using the formula for $\mathbb{G}_{(u)}^{-1}(m+1)$ in (20).

$\mathbf{A}_u^{-1}(m+1)$ and $\mathbf{D}_l^{-1}(m)$ represent common blocks in $\tilde{\mathbb{G}}_M(m)$ as we move from code-block m to $m+1$ and of size $2D \times 2D$ which is a significant overlap with the entire matrix of size $(2D+1) \times (2D+1)$. In what follows, we summarize the complexity involved in computing $\tilde{\mathbb{G}}^{-1}(m+1)$.

- **comp-1**:*Computation of* $\mathbf{\Delta}_l(m)$: $\mathbf{\Delta}_l^{-1}(m)$ is Hermitian and just one block-size B_r. This requires $\frac{B_r^2}{2}$ complex divisions and $\frac{B_r^3}{2}$ complex MAC's.
- **comp-2**:*Computation of* $\mathbf{D}_l^{-1}(m)$: the computation of $\mathbf{Q}_l^H(m)\mathbf{\Delta}_l(m)$ involves $2D$ block MAC's. After this, we compute $\mathbf{Q}_l^H(m)\mathbf{\Delta}_l(m)\mathbf{Q}_l(m)$ and the resulting matrix has Hermitian blocks. Therefore, we need $D(2D+3)$ block MAC's.
- **comp-3**:*Computation of* $\mathbf{\Delta}_u^{-1}(m+1)$: we use the formula $\mathbf{\Delta}_u^{-1}(m+1) = \mathbf{B}_u^H(m+1)\mathbf{A}_u^{-1}(m+1)\mathbf{B}_u(m+1))$ since $\mathbf{C}_u(m+1) = \mathbf{B}_u^H(m+1)$ and we utilize $\mathbf{A}_u^{-1}(m+1) = \mathbf{D}_l^{-1}(m)$. Considering the Hemitian nature of $\mathbf{A}_u^{-1}(m+1)$, this requires $D(2D+3)$ block MAC operations.
- **comp-4**:*Computation of* $\mathbf{Q}_u(m+1)$: we use the formula $\mathbf{Q}_u(m+1) = \mathbf{A}_u^{-1}(m+1)\mathbf{B}_u(m+1)\mathbf{\Delta}_u^{-1}(m+1)$, where $\mathbf{A}_u^{-1}(m+1)\mathbf{B}_u(m+1)$ is available from **comp-3**. The rest of the computations require $2D$ block MAC's.
- **comp-5**:*Computation of* $\mathbf{P}_u(m+1)$: from (20), it is not hard to see that $\mathbf{P}_u(m+1) = \mathbf{A}_u^{-1}(m+1) + \mathbf{Q}_u(m+1)\mathbf{\Delta}_u(m+1)\mathbf{Q}_u^H(m+1)$. The computation of $\mathbf{\Delta}_u(m+1)$ from $\mathbf{\Delta}_u^{-1}(m+1)$ is similar to **comp-1** and the computation of $\mathbf{Q}_u(m+1)\mathbf{\Delta}_u(m+1)\mathbf{Q}_u^H(m+1)$ is similar to **comp-3**

Computations **comp-2,3,4** and **5** require a total of $D(6D+11)$ block MAC's, i.e., $D(6D+11)\frac{B_s^3}{2}$ complex MAC's. Computations **comp-1** and **5** require a total of B_r^3 complex MAC's and B_r^2 complex divisions. Therefore, overall we need to compute $(6D^2+11D+2)\frac{B_r^3}{2}$ complex MAC's and B_r^2 complex divisions.

C. Exploiting the Structure of the Alamouti Block Matrix

Finally, we exploit an interesting property of a matrix with Alamouti blocks; namely, the multiplication and inversion complexity is proportional to the number of Alamouti block rows/columns and not the actual size of the matrix. Given a matrix with Alamouti blocks, we can perform block Gaussian elimination, with each complex division replaced by an Alamouti matrix inversion (which is trivial) and each complex MAC operation replaced by Alamouti MAC operation. Therefore, a block Alamouti matrix of size $M_r \times M_r$ could be considered to be effectively of size $\frac{M_r}{2} \times \frac{M_r}{2}$ which would require about $(6D^2+11D+2)\frac{M_r^3}{16}$ Alamouti MAC operations to invert it. The Alamouti block has only two distinct elements and hence one Alamouti MAC operation translates to exactly four complex MAC's. The inversion of the Alamouti block matrix requires $(6D^2+11D+2)\frac{B_r^3}{4}$ complex MAC's which is half that of a regular complex $\tilde{\mathbb{G}}_M(m)$. Using similar arguments and the result of Section VII-A, it is easy to show that the Grammain operation requires $(2D+1)(D+1)\frac{B_r B_c}{8}\left(\frac{B_r}{2}+1\right)$ complex MAC operations.

D. Illustration

We illustrate the computation savings in Table I for the SFBC and SM schemes discussed in this paper. In each case,

[3]The $[.]_{(m)}$ notation in (19) and (20) indicates that the quantities in the corresponding matrices are matrix functions of m.

$$\tilde{\mathbb{G}}_M(m) = \begin{bmatrix} \mathbf{A}_u(m) & \mathbf{B}_u(m) \\ \mathbf{C}_u(m) & \mathbf{D}_u(m) \end{bmatrix} = \left[\begin{array}{ccc|c} \times & \cdots & \times & \times \\ \vdots & \ddots & \vdots & \vdots \\ \times & \cdots & \times & \times \\ \hline \times & \cdots & \times & \times \end{array}\right] = \left[\begin{array}{c|ccc} \times & \times & \cdots & \times \\ \hline \times & \times & \cdots & \times \\ \vdots & \vdots & \ddots & \vdots \\ \times & \times & \cdots & \times \end{array}\right] = \begin{bmatrix} \mathbf{A}_l(m) & \mathbf{B}_l(m) \\ \mathbf{C}_l(m) & \mathbf{D}_l(m) \end{bmatrix}, \tag{18}$$

$$\mathbb{G}_{(l)}^{-1}(m) = \begin{bmatrix} \boldsymbol{\Delta}_l^{-1} & -\boldsymbol{\Delta}_l^{-1}\mathbf{B}_l\mathbf{D}_l^{-1} \\ -\mathbf{D}_l^{-1}\mathbf{C}_l\boldsymbol{\Delta}_l^{-1} & \mathbf{D}_l^{-1} + \mathbf{D}_l^{-1}\mathbf{C}_l\boldsymbol{\Delta}_l^{-1}\mathbf{B}_l\mathbf{D}_l^{-1} \end{bmatrix}_{(m)} = \begin{bmatrix} \mathbf{P}_l(m) & \mathbf{Q}_l(m) \\ \mathbf{R}_l(m) & \mathbf{S}_l(m) \end{bmatrix} \tag{19}$$

$$\mathbb{G}_{(u)}^{-1}(m) = \begin{bmatrix} \mathbf{A}_u^{-1} + \mathbf{A}_u^{-1}\mathbf{B}_u\boldsymbol{\Delta}_u^{-1}\mathbf{C}_u\mathbf{A}_u^{-1} & -\mathbf{A}_u^{-1}\mathbf{B}_u\boldsymbol{\Delta}_u^{-1} \\ -\boldsymbol{\Delta}_u^{-1}\mathbf{C}_u\mathbf{A}_u^{-1} & \boldsymbol{\Delta}_u^{-1} \end{bmatrix}_{(m)} = \begin{bmatrix} \mathbf{P}_u(m) & \mathbf{Q}_u(m) \\ \mathbf{R}_u(m) & \mathbf{S}_u(m) \end{bmatrix} \tag{20}$$

TABLE I
NUMBER OF COMPUTATIONS IN COMPLEX MAC OPERATIONS

	SFBC-OFDM $B_r \times B_c = 8 \times 4$		SM-OFDM $B_r \times B_c = 4 \times 4$	
	RC	BF	RC	BF
D = 1	638	3228	212	606
D = 2	1611	15380	534	3835

we present the total number of complex MAC operations per symbol using reduced-complexity (RC) and brute-force (BF) approaches. It turns out that the complexity is smaller for SM-OFDM. This is because in the presence of I/Q imbalance and mobility, the sufficient statistic for decoding an SM code block is available in only $2(2D+1)$ sub-carriers whereas that for SFBC is available in $4(2D+1)$ sub-carriers. Moreover, the savings achieved by resorting to the RC approach are much higher for SFBC in comparison to the SM case and this is due to the Alamouti code structure.

VIII. SIMULATION RESULTS

A. Simulation Setup

The system parameters are similar to the 512 sub-carrier profile of the 802.16e mobile WiMAX standard [19], i.e., the bandwidth is 5 MHz, the sampling frequency is 5.6 MHz and the carrier frequency is 2.5 GHz. The channel code used is rate-$\frac{1}{2}$ convolutional code (171,133) with random bit interleaving. We use a frame structure with four OFDM data symbols with embedded pilots, a preamble and a postamble. The pilot overhead ratio of $\frac{1}{7}$, which is the same as that of the Partial Usage of Sub-Carriers (PUSC) mode of the WiMAX standard, but their locations are based on the pilot pattern shown in Figs. 3(a) and 3(b). For SFBC, the parameter L is set to be six. Unless stated otherwise, the following settings are used for the simulations. The channel's power delay profile is the SUI-3 specification with mobility implemented using the Jakes model. A normalized Doppler spread of 2% corresponding to a vehicle speed of 100 km/h is used. The FI I/Q imbalance parameters used are $\alpha_t = \alpha_r = 0.5$ dB, $\theta_t = \theta_r = 5^\circ$. When there is FD I/Q imbalance, the I and Q filters are $\bar{\xi}_r^I(n) = \bar{\xi}_t^I(n) = \delta(n) + 0.1\delta(n-1)$ and $\bar{\xi}_r^Q(n) = \bar{\xi}_t^Q(n) = \delta(n) - 0.1\delta(n-1)$, respectively. At the detector output, soft bit-likelihood ratios are computed which are further processed by the deinterleaver and Viterbi decoder. When pilots are used, they are boosted in power by 2.5 dB than the data sub-carriers in accordance with the 802.16e standard.

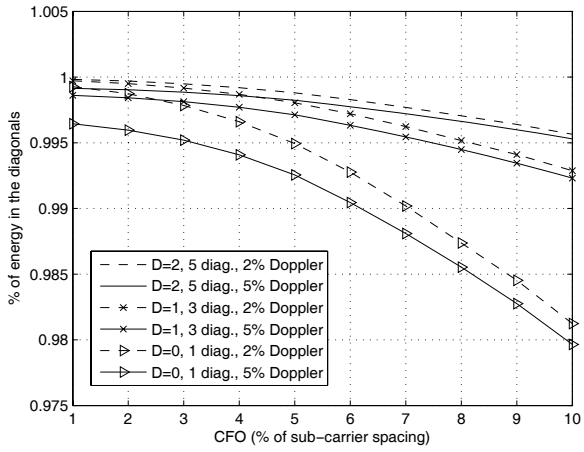

Fig. 4. Energy distribution in the diagonals of the channel matrix for different Doppler values and residual CFO levels.

Finally, in order to perform the MMSE compensation, we need to fix the value of $Q = 2D+1$, the number of block diagonals in the channel matrix or the numbers of taps needed for equalization. Shown in Fig. 4 are the energies in the diagonals of the channel matrix for different Doppler and CFO values. The ordinate is the percentage of energy contained in a given number of diagonals against the entire energy in the channel matrix. The higher this value, the better is the banded approximation. Fig. 4 reveals that $Q = 3$ is sufficient since going from $Q = 3$ to $Q = 5$ results in a very small increase in the percentage of energy.

B. Results and Discussion

Fig. 5 depicts the BER results for Alamouti SFBC-OFDM with $N_P = 1$. BER performance curves for SM-OFDM are shown in Fig. 6 for $N_P = N_Q = 2$. In each case, we present results for uncompensated impariments, compensated with perfect and estimated channel state information (CSI) and the ideal case of no impairments. It can be seen that the uncompensated case exhibits a high error floor and the proposed MMSE compensation helps reducing the error floor by several orders of magnitude. With perfect CSI, the performance comes very close to the case of no impairments though it is not exactly there because we use only $(2D+1)$ main diagonals of the channel. For the estimated CSI case, the performance is within 1 to 2 dB from the case of perfect CSI compensation.

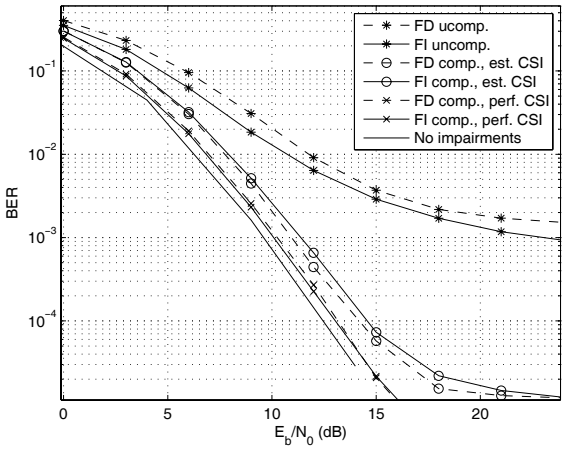

Fig. 5. BER performance of Alamouti SFBC-OFDM using 16-QAM with FI and FD I/Q imbalances and mobility ($\alpha_r = \alpha_t = 0.5$ dB, $\theta_r = \theta_t = 5^\circ$, $\bar{\xi}_r^I(n) = \bar{\xi}_t^I(n) = \delta(n) + 0.1\delta(n-1)$, $\bar{\xi}_r^Q(n) = \bar{\xi}_t^Q(n) = \delta(n) - 0.1\delta(n-1)$, Doppler=2% of sub-carrier spacing).

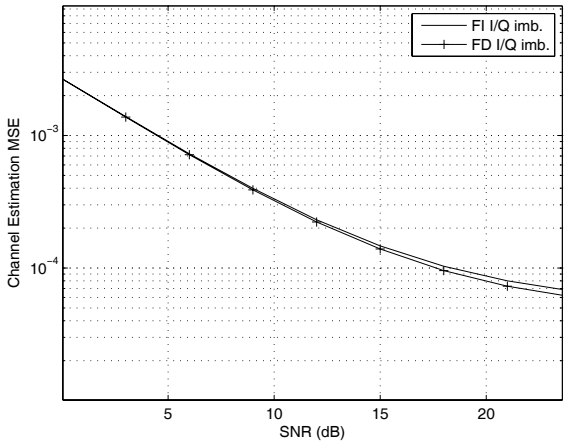

Fig. 7. Channel estimation MSE for SFBC with FI and FD I/Q imbalances and mobility($\alpha_r = \alpha_t = 0.5$ dB, $\theta_r = \theta_t = 5^\circ$, $\bar{\xi}_r^I(n) = \bar{\xi}_t^I(n) = \delta(n) + 0.1\delta(n-1)$, $\bar{\xi}_r^Q(n) = \bar{\xi}_t^Q(n) = \delta(n) - 0.1\delta(n-1)$, Doppler=2% of sub-carrier spacing).

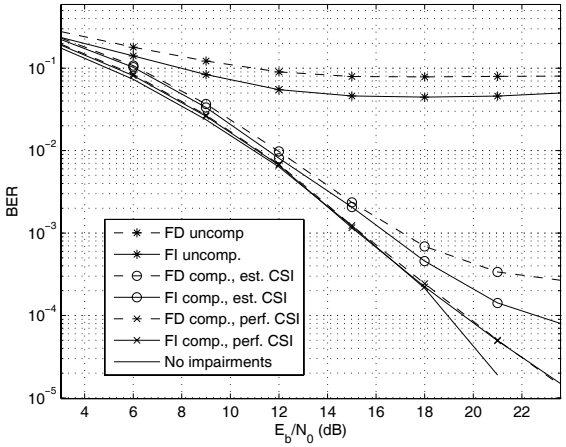

Fig. 6. BER performance of SM-OFDM using 16-QAM with FI and FD I/Q imbalances and mobility ($\alpha_r = \alpha_t = 0.5$ dB, $\theta_r = \theta_t = 5^\circ$, $\bar{\xi}_r^I(n) = \bar{\xi}_t^I(n) = \delta(n) + 0.1\delta(n-1)$, $\bar{\xi}_r^Q(n) = \bar{\xi}_t^Q(n) = \delta(n) - 0.1\delta(n-1)$, Doppler=2% of sub-carrier spacing).

Moreover, in Fig. 7, we have plotted the mean square error (MSE) of channel estimation against SNR for the SFBC case.

Next, we compare the performance of SFBC and SM for different channel delay spreads. The performance of SFBC is sensitive to delay spread because the super-block structure requires the channel response to be constant over $L + D$ sub-carriers. When delay spread is large (i.e., small channel coherence bandwidth), L should be small, but it results in high pilot density $D/(L + D)$, suggesting a tradeoff. For a fair comparison, we consider $N_P = N_Q = 2$ for both SM and SFBC systems. Moreover, SFBC and SM employ 16-QAM and 4-QAM modulation, respectively, to match rates. Severe impairment conditions wherein $\alpha_t = \alpha_r = 0.5$ dB, $\theta_t = \theta_r = 5^\circ$ and a Doppler of 5% (corresponding to a vehicle speed of 235 km/h) were imposed. Both schemes are simulated under SUI-3 and SUI-4 channels which have delay spreads of 0.9 and 4 microseconds, respectively. As is evident from the results in Fig. 8, the Alamouti SFBC performs better when the channel delay spread is small and SM performs better when the delay spread is large.

Now, we demonstrate the robustness of our proposed compensation schemes in the presence of residual CFO in Fig. 9, where we perform the compensation and channel estimation without any modifications to the schemes described in Sections IV and V. For up to 2% CFO, we see that both SFBC and SM exhibit graceful degradation even with $Q = 3$. Finally, in Fig. 10, we show the results for a 64-QAM system where the compensation gains are evident in this case as well. It is worth mentioning that we have not considered the effect of transmit power amplifier (PA) non-linearity in this work. There exist several approaches in the literature to deal with the PA non-linearity such as pre-compensation at the transmitter. However, its effect on IQ imbalance compensation is unclear, and joint compensation of PA non-linearity and I/Q imbalance at the receiver is of practical interest for future research.

IX. Conclusions

In this paper, we proposed reduced-complexity digital baseband estimation and compensation schemes for SM-OFDM and SFBC-OFDM in the presence of I/Q imbalance and high mobility. In each case, generalized linear models were derived for frequency-dependent I/Q imbalance at both the transmitter and receiver in the presence of high mobility. Channel estimation was performed by designing orthogonal pilots in such a way that the I/Q imbalance and channel parameters can be jointly estimated for each transmit-receive antenna pair separately. The channel estimation and compensation schemes remain unchanged irrespective of whether there is I/Q imbalance at the transmitter side only, receiver side only or both and whether the imbalance is frequency-dependent or independent. Using simulations for the WiMAX environment, we showed that if left uncompensated for, I/Q imbalance and mobility result in high error floors and our compensation schemes are effective in reducing these error

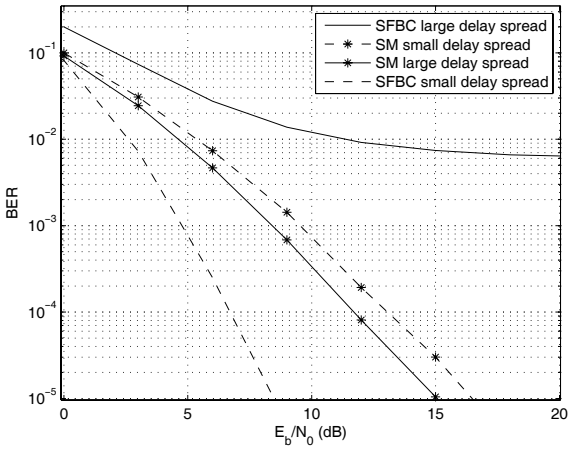

Fig. 8. BER performance comparison of SFBC-OFDM (16-QAM) and SM-OFDM (4-QAM) under different channel delay spreads ($\alpha_r = \alpha_t = 1$ dB, $\theta_r = \theta_t = 10^\circ$, Doppler=5% of sub-carrier spacing).

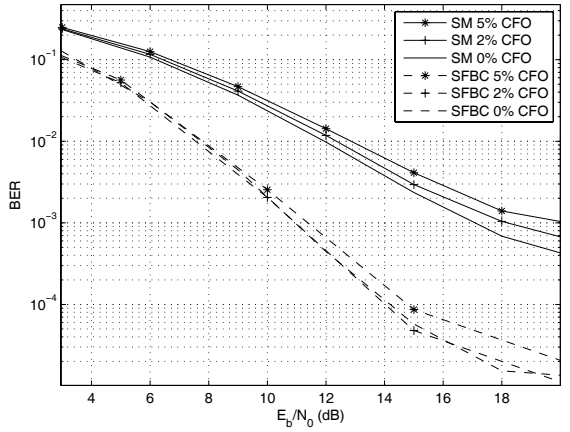

Fig. 9. Performance of 16-QAM SFBC and 16-QAM SM-OFDM scheme with CFO with channel estimation (FI I/Q imbalance $\alpha_r = \alpha_t = 0.5$ dB, $\theta_r = \theta_t = 5^\circ$, Doppler=2% of sub-carrier spacing).

floors significantly. Moreover, our high-mobility simulations showed that SFBC-OFDM outperforms SM-OFDM in the presence of I/Q imbalance with linear MMSE decoding under low channel delay spreads, whereas under high delay spreads, SM performs better at the same pilot density. Finally, we showed how to reduce the computational complexity of the linear MMSE receivers by exploiting the special structure of the matrices involved. For Alamouti SFBC-OFDM, additional reductions in complexity are achievable due to the Alamouti block structure, however, SM-OFDM has lower overall linear MMSE decoding complexity.

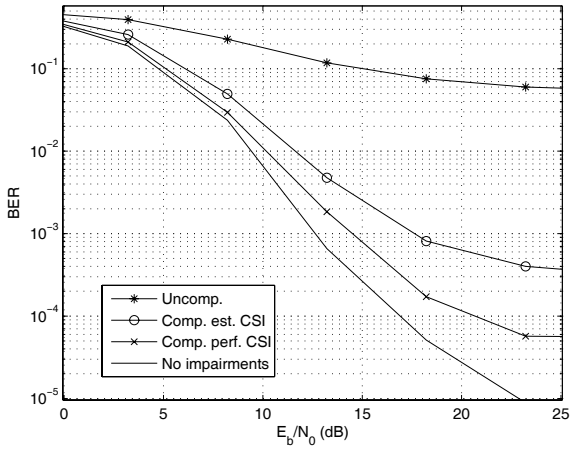

Fig. 10. Performance of 64-QAM SFBC-OFDM scheme with channel estimation (FI I/Q imbalance $\alpha_r = \alpha_t = 0.5$ dB, $\theta_r = \theta_t = 5^\circ$, $\bar{\xi}_r^I(n) = \bar{\xi}_t^I(n) = \delta(n) + 0.1\delta(n-1)$, $\bar{\xi}_r^Q(n) = \bar{\xi}_t^Q(n) = \delta(n) - 0.1\delta(n-1)$, Doppler=2% of sub-carrier spacing, CFO=1%).

REFERENCES

[1] B. Narasimhan, D. Wang, S. Narayanan, H. Minn, and N. Al-Dhahir, "Digital compensation of frequency-dependent joint Tx/Rx I/Q imbalance in OFDM systems under high mobility," vol. 3, no. 3, pp. 405-417, June 2009.

[2] A. Tarighat and A. H. Sayed, "MIMO OFDM receivers for systems with IQ imbalances," *IEEE Trans. Signal Process.*, vol. 53, no. 9, pp. 3583-3595, Sep. 2005.

[3] Y. Zou, M. Valkama, and M. Renfors, "Analysis and compensation of transmitter and receiver I/Q imbalances in space-time coded multiantenna OFDM systems," *EURASIP J. Wireless Commun. Netw.*, vol. 2008, no. 391025, 2008.

[4] D. Tandur and M. Moonen, "STBC MIMO OFDM systems with implementation impairments," in *IEEE VTC 2008-Fall*, Sep. 2008, pp. 1–5.

[5] H. Kamata, K. Sakaguchi, and K. Araki, "An effective IQ imbalance compensation schmeme for MIMO OFDM communication system," in *Proc. IEEE ICC*, June 2006, pp. 251-256.

[6] T. C. W. Schenk, P. F. M. Smulders, and E. R. Fledderus, "Estimation and compensation of Tx and Rx IQ imbalance in OFDM-based MIMO systems," in *Proc. IEEE Radio Wireless Symp.*, Jan. 2006, pp. 215-218.

[7] ——, "Estimation and compensation of frequency selective Tx and Rx IQ imbalance in OFDM-based MIMO systems," in *Proc. IEEE ICC*, June 2006, pp. 251-256.

[8] D. Tandur and M. Moonen, "Compensation of RF impairments in MIMO-OFDM systems," in *Proc. IEEE ICASSP*, Apr. 2008, pp. 3097-3100.

[9] Y.-H. Chung and S.-M. Phoong, "Joint estimation of I/Q imbalance and channel response for MIMO OFDM system," in *Proc. EUSIPCO*, 2007, pp. 906-910.

[10] I. Barhumi and M. Moonen, "Frequency domain IQ imbalance and carrier frequency offset compensation for OFDM over doubly selective channels," in *Proc. European Signal Processing Conf.*, Sep. 2006, pp. 3097-3100.

[11] V. Tarokh, H. Jafarkhani, and A. R. Calderbank, "Space-time block codes from orthogonal designs," *IEEE Trans. Inf. Theory*, vol. 45, no. 5, pp. 1456-1467, July 1999.

[12] S. Lu, B. Narasimhan, and N. Al-Dhahir, "Reduced-complexity ICI mitigation for mobile SFBC-OFDM with application to DVB-H," in *Proc. IEEE WCNC*, Mar. 2008, pp. 1183-1187.

[13] H. Minn and N. Al-Dhahir, "Optimal training signals for MIMO OFDM channel estimation," *IEEE Trans. Wireless Commun.*, vol. 5, no. 5, pp. 1158-1168, May 2006.

[14] S. Kay, *Fundamentals of Statistical Signal Processing: Estimation Theory*. Prentice Hall PTR, 1993.

[15] Y. Mostofi and D. C. Cox, "ICI mitigation for pilot-aided OFDM mobile systems," *IEEE Trans. Wireless Commun.*, vol. 4, pp. 765-774, Mar. 2005.

[16] P. H. Moose, "A technique for orthogonal frequency division multiplexing frequency offset correction," *IEEE Trans. Commun.*, vol. 42, no. 10, pp. 2908-2914, Oct. 1994.

[17] G. Strang, *Linear Algebra and its Applications*, 3rd edition. Harcourt Brace Jovanovich, Inc., 1988.

[18] T. Kailath, A. H. Sayed, and B. Hassibi, *Linear Estimation*. Prentice Hall PTR, 2000.

[19] IEEE Std 802.16e-2005 and IEEE Std 802.16-2004/Cor1-2005, Feb. 2006.